



■ Diiron Complexes

Structural and Electronic Responses to the Three Redox Levels of Fe(NO)N₂S₂-Fe(NO)₂

Pokhraj Ghosh⁺,^[a] Shengda Ding⁺,^[a] Manuel Quiroz⁺,^[a] Nattamai Bhuvanesh,^[a] Chung-Hung Hsieh,^[b] Philip M. Palacios,^[c] Brad S. Pierce,^{*[c]} Marcetta Y. Darensbourg,^{*[a]} and Michael B. Hall^{*[a]}

Abstract: The nitrosylated diiron complexes, Fe₂(NO)₃, of this study are interpreted as a mono-nitrosyl Fe(NO) unit, MNIU, within an N₂S₂ ligand field that serves as a metallodithiolate ligand to a dinitrosyl iron unit, DNIU. The cationic Fe(NO)N₂S₂·Fe(NO)₂⁺ complex, **1**⁺, of Enemark–Feltham electronic notation {Fe(NO)}⁷-{Fe(NO)₂}⁹, is readily obtained via myriad synthetic routes, and shown to be spin coupled and diamagnetic. Its singly and doubly reduced forms, $\{Fe(NO)\}^7 - \{Fe(NO)_2\}^{10}, \quad \mathbf{1}^0, \quad \text{and} \quad \{Fe(NO)\}^8 - \{Fe(NO)_2\}^{10}, \quad \mathbf{1}^-,$ were isolated and characterized. While structural parameters of the DNIU are largely unaffected by redox levels, the MNIU readily responds; the neutral, $S = \frac{1}{2}$, complex, 1°, finds the extra electron density added into the DNIU affects the adjacent MNIU as seen by the decrease its Fe-N-O angle (from 171° to 149°). In contrast, addition of the second electron, now into the MNIU, returns the Fe-N-O angle to 171° in 1-. Compensating shifts in Femnil distances from the N_2S_2 plane (from 0.518 to 0.551 to 0.851 Å) contribute to the stability of the bimetallic complex. These features are addressed by computational studies which indicate that the MNIU in 1 is a triplet-state {Fe(NO)}⁸ with strong spin polarization in the more linear FeNO unit. Magnetic susceptibility and parallel mode EPR results are consistent with the triplet state assignment.

With its easily accessible one-electron, reduced (NO⁻), and one electron-oxidized (NO⁺) forms, nitric oxide (NO⁻) as a ligand shows extensive electronic interplay in metal-nitrosyl fragments, resulting in considerable structural and bonding intricacies especially in M(NO) and M(NO)₂ units.^[1-4] Complexes containing the dinitrosyl iron units, Fe(NO)₂ or DNIUs, increasingly gain attention as physiologically important products of NO overload or NO storage.^[5,6] Nevertheless, the predominant

chemical relevance of NO in biology stems from various hemetype {Fe(NO)}^{6/7/8} species of distinctive IR and EPR spectral features and solid state metric parameters.^[7] While the {Fe(NO)}⁷ species is most prevalent, rare illustrations of the reduced {Fe(NO)}⁸ have been noted in synthetic porphyrins decorated with electron-withdrawing groups.^[8-11] Examples are also known for non-heme, cyclam-based macrocycles and in a tetracarbene binding scaffold.^[12-15] In the latter, Meyer et al. presented X-ray crystal structures in three redox levels.^[15]

Contiguous N_2S_2 donor sites are efficient and versatile tetradentate ligands, creating MN_2S_2 units whose S-based nucleophilicity has yielded a wide range of di- and poly-heterometal-lic complexes. While mostly explored with $M=Ni^{2+}$, other dications such as $[Fe(NO)]^{2+}$, $[Co(NO)]^{2+}$, and $[V\equiv O]^{2+}$ are also included in this new class of metallo-ligands. A notable biological N_2S_2 site in Acetyl-coA Synthase (ACS) is constructed of a Cys-Gly-Cys tripeptide motif that securely binds a catalytically inactive $Ni^{11}.^{177,18}$ A second, kinetically labile nickel is attached to the NiN_2S_2 moiety via the cis-dithiolate sulfurs, is presumed to orchestrate the C–C coupling processes in ACS.

An ACS-related structure, [Fe(NO)N₂S₂·Fe(NO)₂]^{+/0} was revealed by us during studies of metallodithiolates as ligands in dinitrosyliron complexes, DNICs, Figure 1.^[19] The redox activity of this diiron complex, centered at both iron atoms, and exhibiting two fully reversible electrochemical events, encouraged its exploration as a proton reduction electrocatalyst in mimicry of the [FeFe]-H₂ase active site.^[19-21] Specifically, redox reactivity in the NO of the Fe(NO) unit might mimic the 4Fe4S cluster of the H-cluster. Generally, the diiron complex offers opportunity to examine the mutual influence of redox active units as mediated by sulfur bridges.

As indicated in Figure 1, multiple chemical routes led to the cationic, oxidized form, {Fe(NO)₂}⁷-{Fe(NO)₂}⁹, that is,1⁺ or 1*⁺, implicating particular thermodynamic stability and a self-assembly process. Herein we will give distinguishing properties

[a] P. Ghosh,⁺ S. Ding,⁺ M. Quiroz,⁺ Dr. N. Bhuvanesh, Prof. Dr. M. Y. Darensbourg, Prof. Dr. M. B. Hall Department of Chemistry, Texas A&M University 3255 TAMU, College Station, TX 77843 (USA) E-mail: marcetta@chem.tamu.edu hall@science.tamu.edu

[b] Prof. C.-H. Hsieh Department of Chemistry, Tamkang Univesrity New Taipei City, 25157 (Taiwan)

- [c] P. M. Palacios, Prof. Dr. B. S. Pierce Department of Chemistry, University of Texas at Arlington 503 W 3rd St, Arlington, TX 76010 (USA) E-mail: bspierce@uta.edu
- [+] Contributed equally to this work.
- Supporting information and the ORCID identification number(s) for the author(s) of this article can be found under:
 https://doi.org/10.1002/chem.201804168: Experimental and computational details, synthetic protocol, crystallography data, structure tables, magnetic characterization, and EPR specifics.

16003



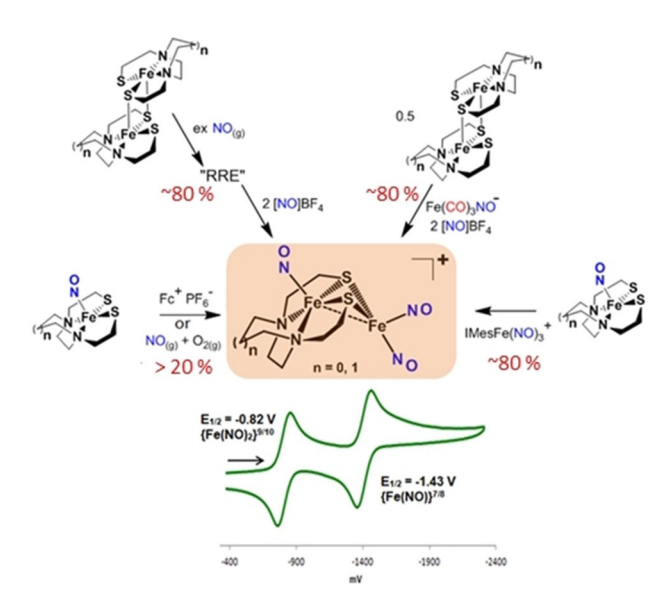


Figure 1. A selection of synthetic routes for the formation of the oxidized diiron-trinitrosyl complex, $Fe(NO)N_2S_2$ · $Fe(NO)_2^+$, with N_2S_2 ligands, bis-mercaptodiazamethyl-ethane, bme-dame $(n\!=\!0)$, complex 1^+ , and bis-mercaptodiazacycloheptane, bme-dach $(n\!=\!1)$, complex 1^{*+} . The cyclic voltammogram of 1^+ was recorded in CH_2CI_2 at a scan rate of 200 mV sec $^{-1}$ and referenced to $Fc^{+/0}\!=\!0.00$ V.

of $\{Fe(NO)\}^{7/8}$ within a diiron complex containing the mononitrosyl in N_2S_2 binding that acts as a metalloligand to a $Fe(NO)_2$ unit, which itself is stable in two redox levels, $\{Fe(NO)_2\}^{9/10}$.

Initial studies of the $[Fe(NO)N_2S_2\cdot Fe(NO)_2]^{+/0}$ construct made use of an N_2S_2 ligand containing a moderately rigid diazamesocycle grafted to bis-mercaptoethylene arms, complexes 1^{*+} and 1^{*0} as indicated in Figure 1. Difficulties in the isolation of the doubly-reduced, anionic 1^{*-} , $\{Fe(NO)\}^8-\{Fe(NO)\}^{10}$, prompted adjustment to a more flexible, open-chain, bmedame (bis-mercaptoethyl-diazamethylethane) ligand, $[2^{22}]$ to prepare the mononitrosyliron complex, (bme-dame)Fe(NO). This MNIC is used as the metallodithiolate ligand in the 1^+ , 1^0 and 1^- complexes of this study.

Synthesis and Characterization

The key precursor to the MNIU of the bimetallic complex is dimeric ([FeN₂S₂]₂), readily cleaved by NO(g). [23] The most selective route to the Fe(NO)N₂S₂·Fe(NO)₂+ complex, three o'clock position in Figure 1, is found to be the reaction of an *N*-heterocyclic-carbene-stabilized, trinitrosyliron complex (TNIC), [(IMes)Fe-(NO)₃]+, [24] with Fe(NO)N₂S₂ as nucleophile, displacing an NO radical, as well as the NHC, to form oxidized diiron complex 1⁺. At one o'clock in Figure 1, the "one-pot" synthesis, involved in situ generation of NO and the putative [Fe(CO)₂(NO)₂]+ to serve as a Fe(NO)₂+ source, [25] derived from [Fe(CO)₃(NO)]- and two equivalents of [NO][BF₄]. The in situ generated NO and Fe(NO)₂+ react with the [FeN₂S₂]₂ dimer to yield the target trinitrosyl bimetallic. Such synthetic

routes, using the bme-dame and bme-dach ligands, gave isolated yields of $\approx 80\,\%$.

In contrast to the reaction of the [FeN₂S₂]₂ dimer with a stoichiometric amount of NO(g) that forms Fe(NO)N₂S₂, addition of excess NO(g), leads to a Roussin's Red Ester (RRE) derivative, [26] indicated by position and separation of the signature v(NO)bands at 1780 and 1754 cm⁻¹. Although this species has not been structurally characterized, it is likely a (precedented) dimeric structure in which two S-N-N-S dithiolate ligands span two RRE units.^[27] Subsequent oxidation of this species by [NO] [BF₄] formed complex 1⁺ or 1*⁺ in \approx 80% yields. Oxidation of the [FeN₂S₂]₂ dimer by aerial O₂, or Fc⁺, in the presence of excess NO(g) also generated 1+ and 1*+, albeit in yields < 20 %. Formation of {Fe(NO)}⁷-{Fe(NO)₂}⁹ was repeatedly observed in various reactivity studies with Fe(NO)N₂S₂, under oxidizing conditions. The isolated yields for these reactions were marginal, as expected from the low atom economy in such circuitous routes. Full experimental descriptions and characterizations are provided in the Supporting Information.

The cyclic voltammogram of complex 1^+ in CH_2CI_2 displayed two-single-electron, fully reversible events at $E_{1/2} = -0.82$ V and -1.43 V, assigned as the $\{Fe(NO)\}^7 - \{Fe(NO)_2\}^{9/10}$, and the $\{Fe(NO)\}^{7/8} - \{Fe(NO)_2\}^{10}$ couples, respectively, Figures 1 and S1. Thus, the reduced species, $\{Fe(NO)\}^7 - \{Fe(NO)_2\}^{10}$ and $\{Fe(NO)\}^8 - \{Fe(NO)_2\}^{10}$, were targeted for isolation. Treatment of 1^+ with 1 equiv of K^+ (or Na^+) HBEt $_3^-$ in THF at 0 °C, showed a color change from dark brown to green with a concomitant blue shift in all three v(NO) stretching frequencies by ca. 110 cm $^{-1}$, Figure 2. The air sensitive neutral compound, 1^0 , was isolated as a green solid by layering a THF solution with pentane.

An extra 1.3 equiv of $K^+HBEt_3^-$ added to 1^0 at $-40\,^{\circ}C$ showed a further, but less dramatic, $30\,\mathrm{cm}^{-1}$ shift in the v(NO) stretching frequencies to lower values, Figure 2. Notably, while the site of reduction is reasonably assigned to the separate components of the $Fe_2(NO)_3$ complex, the three nitrosyls in both reduced levels conjointly respond to the added electrons; the first added electron, largely on the $Fe(NO)_2$, evincing a greater response. The anionic complex, 1^- , was isolated at $\approx -40\,^{\circ}C$ as its $K^+/18$ -Cr-6 salt; reddish-brown plates, suitable for XRD, were obtained from THF/pentane and stored at $-35\,^{\circ}C$.

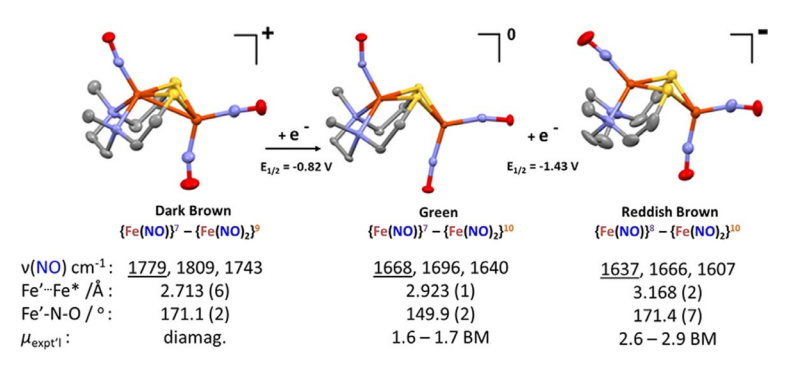


Figure 2. Sequential reduction of 1⁺ to 1⁰ and to 1⁻ withv(NO) IR values (THF solution), and XRD structures (Fe′···Fe* distances and Fe′-N-O angles shown); Fe″ refers to Fe(NO) and Fe* to Fe(NO)₂. Other metric parameters are listed in Table 1 and in the Supporting Information. Magnetic susceptibility and μ_{expt1} determined by Evans method using CF₃C₆H₅ as shift agent.

www.chemeurj.org



CHEMISTRY
A European Journal
Communication

Because of their thermal sensitivity, samples of 1⁻ were generated by quantitative in situ reduction of 1⁰. Figure 2 summarizes the sequential reduction processes, with selected spectral, magnetism, and metric data for the products. Table 1 lists further comparisons and calculated values. Full XRD reports are deposited in the Supporting Information.

Table 1. Comparison of experimental and computed parameters of the $\{Fe(NO)\}^{7/8}$ moieties in 1+, 10 and 1-.

	1+		1º		1-	
multiplicity E–F count d electron configuration	BS singlet $\{Fe(NO)\}^7$ $(d_{z^2})^1(d_{xy})^0$		Doublet $\{Fe(NO)\}^7$ $(d_{z^2})^1(d_{xy})^0$		Triplet $\{Fe(NO)\}^8$ $(d_{z^2})^1(d_{xy})^1$	
Measurable $d(Fe'-N)$ [Å] ^[a] Fe'_{disp} [Å] ^[b] $(N_2S_2)_{dist}$ [Å] ^[c] τ value ^[35]	Expt. 1.666(2) 0.518 0.094 0.18		Expt. 1.709(5) 0.531 0.114 0.21	1.681 0.517 0.103 0.18	Expt. 1.720(7) 0.851 0.058 0.11	calcd 1.728 0.864 0.114 0.20
\(\lambda \text{(Fe'-N-O) [°]} \\ \(\nabla \text{(NO) [cm\$^{-1}]\$}^{[d]} \end{array}	171.1(2) 1779	161.6 1868	149.9(4) 1668	149.4 1734	171.4(7) 1637	170.0 1675

[a] Fe" to N distance in MNIU. [b] The distance between apical Fe" and the mean plane of the N_2S_2 chelating ligand of the MNIC. [c] The (unsigned) average displacement of two sulfur and two nitrogen atoms from the N_2S_2 mean plane. [d] Calculated numbers are unscaled.

EPR Studies

The transverse mode EPR spectra shown in Figure S6 (panel A) confirm that the g=2.024 (S=1/2) species observed for 1° (trace [a]), is abolished upon reduction of the complex. Instead, two new signals are observed with g-values near 2.0, albeit at significantly reduced intensity relative to the starting 1° complex. Both signals follow Curie law behavior and collectively account for <13% of initial 1° concentration. Further discussion of these S=1/2 species is given in the EPR spectroscopy section in the Supporting Information.

As the anticipated spin for 1^- is an integer value (S=1), EPR data were also collected with the microwave polarization parallel to the static magnetic field $(B_1 || B_0)$ using a Bruker bimodal resonator (4116DM). As shown in Figure S6, panel C (trace [d]), a broad signal can be observed in samples of 1- with an observed g-value of 4.0. This signal is consistent with the presence of an S=1 spin-state. [28-29] The temperature-normalized signal intensity shown in Figure S7 illustrates that the greatest intensity occurs at the lowest temperature (4.2 K) and decreases with increasing temperature. Therefore, this transition must originate from within a ground state doublet of a "non-Kramers" center. Within the "good quantum number" regime, [30-33] this is represented by the $|ms> = \pm 1$ eigen states. The value of the axial zero field splitting term ($D = -35 \pm 3 \text{ cm}^{-1}$) was determined by fitting this data to a Boltzmann population distribution for a 2-level system (Figure S7, solid line). Figure S6C (trace [d], dashed line) illustrates the simulated parallel mode EPR spectrum for 1⁻ utilizing the experimental determined Dvalue and a small rhombic distortion near the axial limit (E/D, 0.003). This simulation also includes distributions in E/D ($\sigma_{E/D}=0.02$) in order to accurately reproduce the spectral line width. From this analysis, the concentration of $\mathbf{1}^-$ determined by simulation is 19 ± 5 mm. After subtraction of the afore-mentioned S=1/2 impurities, the calculated concentration of this triplet signal accounts for nearly 90% of the expected $\mathbf{1}^-$ concentration based on mass balance. These studies indicate nearly stoichiometric formation of a triplet spin-state upon reduction of $\mathbf{1}^0$. This conclusion is supported by magnetic susceptibility measurements, which indicate a range of 2.56–2.92 BM for the effective magnetic moment, Figures S8–S9. A summary of all EPR data is provided in Table S1.

X-ray Diffraction Analysis

The molecular structures of the bme-dach analogue of the cationic 1*+ and the neutral, singly reduced 1*0 complexes were reported earlier.^[19] Using the bme-dame N₂S₂ ligand, crystals suitable for X-ray diffraction analysis of 1+, 10 and 1- were obtained; detailed procedures and crystallographic reports are in the Supporting Information, Figures S10–S15 and Tables S2–S5. Selected metric parameters are listed in Figure 2 and Table 1. Note especially the Fe'-N-O angle within the square pyramidal MNIU (τ values of 0.1 to 0.2) increases from the unbound metallodithiolate ligand (ca. 155.2°)^[23] to 171.1° in $\mathbf{1}^{+}$ as electron density is withdrawn on binding to the cationic DNIC unit. Consistent with conventional perception of M-N-O angles, on reduction of the DNIC unit the added electron density found in 1° diminishes the Fe'-N-O angle of the MNIU to 149.9°; the displacement of Fe from the best N₂S₂ plane increases by 0.013 Å. As the second electron is added, and largely localized on the MNIU, vide infra, a much larger Fedisp of 0.32 Å is concomitant with much smaller shifts in v(NO). Notably, the Fe-N-O angle increases in 1⁻, in fact it returns to 171° as seen for 1⁺. That is, the anionic {Fe(NO)}⁸-{Fe(NO)₂}¹⁰ complex showed marked linearity in the Fe'-N-O angle of the MNIU which is a rare example of a high spin, non-heme, linear {Fe(NO)}⁸ species. It is further distinctive in that the reduced iron nitrosyls are adjacent within a diiron complex.

Computational Modeling

Density functional theory (DFT) calculations were applied to 1^+ , 1^0 and 1^- to clarify the electron partitioning between iron and nitrosyl(s), and to correlate this partitioning with the geometric changes, particularly the changes in the Fe'-N-O angle. All energies reported are Gibbs free energy, calculated for CH_2Cl_2 solvation.

The MNIU and DNIU electronic states, energies and structural consequences

Consistent with the diamagnetism of complex 1⁺, computations predict a singlet ground state with the broken-symmetry^[34] (BS) singlet, 2.0 kcal mol⁻¹ more stable than the triplet and 10.0 kcal mol⁻¹ more stable than the closed-shell (CS) singlet. The BS singlet features anti-ferromagnetically coupled



 ${\rm Fe(NO)}^7$ and ${\rm Fe(NO)}_2{\rm P}^9$ spin centers^[19] with the iron atoms separated by 2.834 Å.

Two successive reductions of 1⁺ produce 1⁰ and 1⁻, respectively, with the added electrons assigned to the {Fe(NO)₂}^{9/10} and the {Fe(NO)}^{7/8} moieties, respectively. In agreement with the experimental results, the calculations show that complex 1º is a doublet with one unpaired electron in the {Fe(NO)}⁷ moiety, while complex 1 is a triplet, with two unpaired electrons in the {Fe(NO)}⁸ unit. The calculations also corroborate changes in the Fe-N-O angle: 170.0° (expt.: 171.4°) in 1-, 149.4° (expt.: 149.9°) in **1**°, and 161.6° (expt.: 171.2°) in **1**⁺. The SP structure of the Fe(NO)(N₂S₂) fragment is maintained throughout the three redox levels (τ values^[35] in Table 1). The largely linear {Fe(NO)}⁸ moiety in square pyramidal geometry is reproduced, along with the displacement of Fe from the mean N_2S_2 plane: 0.864 Å (expt.: 0.851 Å) in 1⁻, 0.517 Å (expt.: 0.531 Å) in 1°, and 0.515 Å (expt.: 0.518 Å) in 1+. The Fe'-N-O angle and the ${\rm Fe'}_{\rm disp}$ are closely coupled and related to the electronic structures of 1+, 10 and 1-, vide infra.

The {Fe(NO)}⁷ moiety in 1⁺ and 1⁰ have one unpaired electron in the d_{z^2} orbital with a d-configuration of $(d_{x^2-y^2})^2(d_{xz})^2(d_{yz})^2(d_{z^2})^1(d_{xy})^{0.[36]}$ (The electrons are arbitrarily assigned to the iron regardless of the electron partitioning between Fe and NO; note the coordinate definition in Figure 3C.) In the subsequent reduction of 1°, the incoming electron is added to the Fe(NO) fragment's d_{xy} orbital, that is, the antibonding orbital from N_2S_2 σ -donations. This reduction results in an overall configuration of $(d_{x^2-y^2})^2(d_{xz})^2(d_{yz})^2(d_{zz})^1(d_{xy})^1$ in the $\{Fe(NO)\}^8$ moiety of 1⁻. The d_{xy} has no direct overlap with the nitrosyl, this assignment justifies the small shift of NO vibrational frequency of the Fe(NO) moiety, 59 cm⁻¹ (expt.: 31 cm⁻¹) after reduction of 1°, in contrast to the shift of the mononitrosyl by $134~\text{cm}^{-1}$ (expt.: $111~\text{cm}^{-1}$), from 1^+ to 1^0 given that the reduction happens on the {Fe(NO)₂} moiety. However, because the d_{xv} is strongly destabilized, the Fe(NO) system further changes its structure to better accommodate the added electron; see next Section.

Spin Polarization, Orbital Overlap in π -Back-Bonding and the Interplay between Electronic and Geometric Structures

Although the unpaired electron on the 1° is formally on the iron of the {Fe(NO)}⁷ moiety, the spin polarizes such that both iron atoms share the same spin alignment, Figure 3 A. For the {Fe(NO)}⁸ moiety of 1⁻, significant spin polarization (Figure 3 B, also see Figure S16) occurs in the π -back-bonding orbitals formed by the overlap of the d_{xz} and d_{vz} orbitals on Fe and the $2\pi_x$ and $2\pi_v$ orbitals of NO, such that the Fe's spin density is 3.0, while the spin density of its NO is -1.2. Although the {Fe(NO)₂}¹⁰ moiety is saturated, it also shows Fe/NO spin-polarization (Figure 3B) as well. Such spin-polarization indicates that the nitrosyls withdraw electron density, of one spin preferably, from the iron atoms to stabilize the electron-rich system and the electrons of the opposite spin localize on each iron to take advantage of iron's high exchange energy. The corresponding singlet of 1⁻, which eliminates the spin-polarization and pairs the two above-mentioned unpaired electrons in the

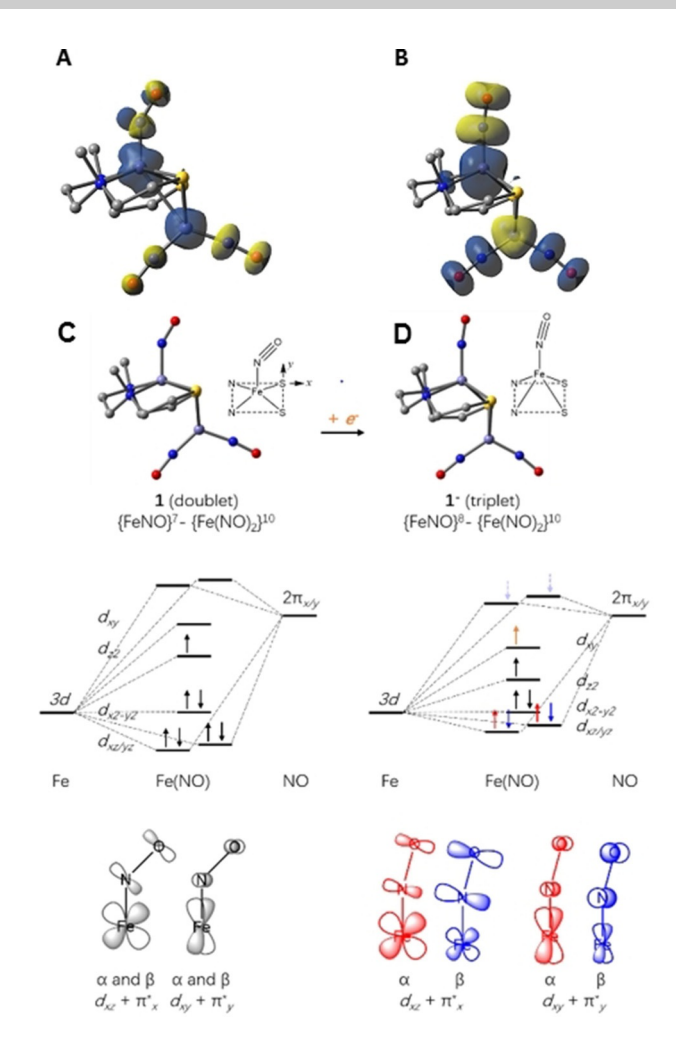


Figure 3. Spin density plots (isovalue = 0.005 a.u.) of A) 1^{0} and B) 1^{-} ; C),D) The geometric and electronic structure changes after the reduction of 1^{0} into 1^{-} .

 d_{z^2} orbital of the $\{Fe(NO)\}^8$ unit, is 16.5 kcal mol $^{-1}$ higher than the triplet.

Figure 4 sketches how individual d orbitals of a metal in the SP geometry interact with orbitals of an axial NO and their geometric preferences.³² The d_{xz} , d_{yz} orbitals, if occupied, prefer a linear NO (180°) to maximize their π -back-bonding. Such a linear structure also helps the NO donate electron density from its 5σ into the iron's d_{z^2} , should it be empty. In contrast, a doubly-occupied d_{z^2} would benefit from a bend in the NO, typically 120° - 130° for the doubly-occupied d_{z^2} , so that the over-

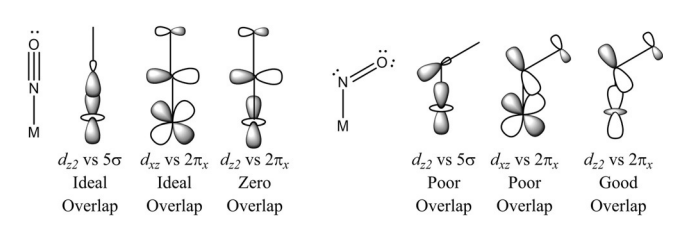


Figure 4. Fe'-N-O angle preferences of individual d orbitals with sketches of orbital overlap.





lap between d_{z^2} and NO's 2π can be established to conduct σ back-bonding. In addition, this bending of NO also helps stagger the occupied d_{z^2} away from NO's 5σ donor orbital. The same preference, though less prominent, is applicable to a singly occupied d_{z^2} .

The cationic 1⁺ and neutral 1⁰, featuring a {Fe(NO)}⁷ unit with only one electron in d_{z^2} and no electrons on d_{xw} show subtle changes of the Fe-N-O angle. In 1+, the singly occupied d_{z2} would prefer a bent Fe-N-O angle. However, it is spin paired with the electron on the {Fe(NO)₂}⁹ and delocalizes away from the attached NO, which results in a wider angle of 161.6° (expt.: 171.1°). The incoming electron in the reduction of 1⁺ is accepted by the {Fe(NO)₂}⁹ moiety, which eliminates the spin-pairing between two iron atoms and, in response, the now more electron rich {Fe(NO)}⁷ bends the Fe-N-O angle to 149.4° (expt.: 149.9°). When the next electron is added to the high-lying d_{xy} of 1° , the Fe moves further out of the N_2S_2 plane by 0.347 Å (expt. 0.32 Å) with elongated Fe-N(N₂S₂) and Fe- $S(N_2S_2)$ bond lengths to stabilize the d_{xy} orbital. The NO also responds to the now elevated electron density in the {Fe(NO)}⁸ moiety of 1⁻ by restoring a more linear Fe-N-O angle (170.0°, expt.: 171.4°), which helps achieve the maximal back-bonding from the doubly occupied d_{xz} and d_{yz} instead of the singly occupied d_{z^2} , and relieve the electron crowdedness on the iron. Significant spin-polarization was observed between Fe and NO as part of the efforts to stabilize the electron-rich system, Figure 3B. It verifies the idea that the d orbital preference over the Fe-N-O angle (Figure 4) is biased by its occupancy number. The computationally modelled singlet state 1 with doubly occupied d_{z^2} and vacant d_{xw} shows a sharply bent Fe-N-O angle of 131.0° and a smaller Fe displacement from the N₂S₂ plane (0.585 Å, as compared to 0.864 Å of the triplet). Many {Co(NO)}⁸ moieties inscribed in SP environments prefer a doubly occupied d_{z^2} (i.e. the same configuration as singlet {Fe(NO)}⁸) and were experimentally characterized to have bent Co-N-O.[37]

Comments on Another Linear Singlet {Fe(NO)}⁸ System

There could be additional factors stabilizing the $\{M(NO)\}^n$ moieties. A linear (169.1°) singlet $\{Fe(NO)\}^8$ moiety in the SP environment was reported in 2016 by DeBeers, Meyer and coworkers. Their Fe(NO) is coordinated by four equatorial carbene carbons from a cyclic chelating (NHC)₄ ligand. On reproducing their calculations, we found the doubly occupied d_{z^2} orbital is stabilized by π^* orbitals of the four *N*-heterocarbenes, which tilt below the equatorial plane to achieve orbital overlap, Figure S17. Because of this stabilization of the d_{z^2} , the 2π orbitals of NO interact exclusively with the d_{xz} , d_{yz} orbitals, which lead to a linear Fe-*N*-O angle, despite the singlet configuration.

Remarks

The isolation and characterization of three redox levels of a diirontrinitrosyl complex, $1^{+/0/-}$, has revealed important and unanticipated structural changes of the Fe(NO) fragment

www.chemeurj.org

during redox events. The XRD analysis, solid-state structures, and IR data are consistent with data from EPR spectroscopy, magnetic susceptibility and computational modeling that define the electronic structures of these species. The iron atoms and their bound nitrosyls are capable of reorganizing their orbitals in cooperative structural alterations, and subtle tuning of back-bonding to the NO's so as to rebalance the electron density. The intriguing interplay again emphasizes the role of the π -acid ligand, nitrosyl, as a buffer of electrons. It is noteworthy that the bimetallic 1+ and 1*+ are electrocatalysts for H₂ generation; in this regard, the electron buffering capacity of NO was earlier highlighted in the details of our mechanistic study.[19-21] We introduced NO into models of the [FeFe]-hydrogenase enzyme active site with the expectation that it might reproduce the function of the electron reservoir [Fe₄S₄]sub-cluster in the H-cluster. Clearly the binding capability of the N₂S₂ unit to both Fe(NO) and Fe(NO)₂ persists through two reductions increasing the overall electron count by two. The burden of the redox changes is shared throughout the nitrosylated iron complex, including shifts in the orientation of the N₂S₂ ligand donor orbitals. These results emphasize the importance of the holistic or entire molecular framework.

Acknowledgements

We appreciate financial support from the National Science Foundation (CHE-1665258 to M.Y.D., and CHE-1300787, CHE-1664866 to M.B.H.), the Robert A. Welch Foundation (A-0924 to M.Y.D., and A-0648 to M.B.H.), the National Institute of Health (NIGMS, GM117511-01 to B.S.P.) and the National Science Foundation (CHE, 1709369 to B.S.P.). The authors acknowledge the Laboratory for Molecular Simulation at Texas A&M University for providing computing resources.

Conflict of interest

The authors declare no conflict of interest.

Keywords: diiron \cdot electron buffer \cdot EPR \cdot metallodithiolate ligand \cdot nitric oxide \cdot redox levels

- [1] J. H. Enemark, R. D. Feltham, Coord. Chem. Rev. 1974, 13, 339 406.
- [2] R. Hoffmann, M. M. L. Chen, D. L. Thorn, *Inorg. Chem.* 1977, 16, 503–511.
- [3] S. Ye, F. Neese, J. Am. Chem. Soc. 2010, 132, 3646 3647.
- [4] C. Hauser, T. Glaser, E. Bill, T. Weyhermüller, K. Wieghardt, J. Am. Chem. Soc. 2000, 122, 4352–4365.
- [5] A. F. Vanin, *Bioorganometallic Chemistry*, Wiley-VCH, Weinheim (Germany), 2015, pp. 203 238.
- [6] J. R. Hickok, S. Sahni, H. Shen, A. Arvind, C. Antoniou, L. W. M. Fung, D. D. Thomas, Free Radical Biol. Med. 2011, 51, 1558 – 1566.
- [7] G. R. A. Wyllie, W. R. Scheidt, Chem. Rev. 2002, 102, 1067 1090.
- [8] J. Pellegrino, S. E. Bari, D. E. Bikiel, F. Doctorovich, J. Am. Chem. Soc. 2010, 132, 989–995.
- [9] L. E. Goodrich, S. Roy, E. E. Alp, J. Zhao, M. Y. Hu, N. Lehnert, *Inorg. Chem.* 2013, 52, 7766–7780.
- [10] B. Hu, J. Li, Angew. Chem. Int. Ed. 2015, 54, 10579–10582; Angew. Chem. 2015, 127, 10725–10728.





- [11] N. Kundakarla, S. Lindeman, M. H. Rahman, M. D. Ryan, *Inorg. Chem.* 2016, 55, 2070 – 2075.
- [12] R. G. Serres, C. A. Grapperhaus, E. Bothe, E. Bill, T. Weyhermüller, F. Neese, K. Wieghardt, J. Am. Chem. Soc. 2004, 126, 5138-5153.
- [13] S. Speelman, N. Lehnert, Angew. Chem. Int. Ed. 2013, 52, 12283 11228; Angew. Chem. 2013, 125, 12509 – 12513.
- [14] A. M. Confer, A. C. McQuilken, H. Matsumura, P. Moënne-Loccoz, D. P. Goldberg, J. Am. Chem. Soc. 2017, 139, 10621 10624.
- [15] C. Kupper, J. A. Rees, S. Dechert, S. DeBeer, F. Meyer, J. Am. Chem. Soc. 2016, 138, 7888–7898.
- [16] J. A. Denny, M. Y. Darensbourg, Chem. Rev. 2015, 115, 5248 5273.
- [17] M. Can, F. A. Armstrong, S. W. Ragsdale, Chem. Rev. 2014, 114, 4149–4174.
- [18] C. Darnault, A. Volbeda, E. J. Kim, P. Legrand, X. Vernede, P. A. Lindahl, Nat. Struct. Mol. Biol. 2003, 10, 271 – 279.
- [19] C.-H. Hsieh, S. Ding, Ö. F. Erdem, D. J. Crouthers, T. Liu, C. C. L. McCrory, W. Lubitz, C. V. Popescu, J. H. Reibenspies, M. B. Hall, M. Y. Darensbourg, *Nat. Commun.* 2014, 5, 3684.
- [20] S. Ding, P. Ghosh, M. Y. Darensbourg, M. B. Hall, Proc. Natl. Acad. Sci. USA 2017, 114, E9775 – E9782.
- [21] P. Ghosh, S. Ding, R. B. Chupik, C.-H. Hsieh, M. Quiroz, N. Bhuvanesh, M. B. Hall, M. Y. Darensbourg, Chem. Sci. 2017, 8, 8291 – 8300.
- [22] K. D. Karlin, S. J. Lippard, J. Am. Chem. Soc. 1976, 98, 6951 6957.
- [23] K. D. Karlin, H. N. Rabinowitz, D. L. Lewis, S. J. Lippard, *Inorg. Chem.* 1977, 16, 3262–3267.
- [24] C.-H. Hsieh, M. Y. Darensbourg, J. Am. Chem. Soc. 2010, 132, 14118– 14125.

- [25] C. H. Hsieh, S. M. Brothers, J. H. Reibenspies, M. B. Hall, C. V. Popescu, M. Y. Darensbourg, *Inorg. Chem.* 2013, 52, 2119 – 2124.
- [26] A. R. Butler, Chem. Rev. 2002, 102, 1155-1165.
- [27] C.-Y. Chiang, M. L. Miller, J. H. Reibenspies, M. Y. Darensbourg, J. Am. Chem. Soc. 2004, 126, 10867 – 10874.
- [28] C. C. Tannoudji, Quantum Mechanics, Wiley, New York, 1977.
- [29] A. Abragam, B. Bleaney, Electron paramagnetic resonance of transition ions, Oxford University Press, New York, 1970.
- [30] R. Gupta, D. C. Lacy, E. L. Bominaar, A. S. Borovik, M. P. Hendrich, J. Am. Chem. Soc. 2012, 134, 9775–9784.
- [31] M. P. Hendrich, P. G. Debrunner, Biophys. J. 1989, 56, 489-506.
- [32] M. P. Hendrich, E. Munck, B. G. Fox, J. D. Lipscomb, J. Am. Chem. Soc. 1990, 112, 5861 – 5865.
- [33] D. C. Lacy, R. Gupta, K. L. Stone, J. Greaves, J. W. Ziller, M. P. Hendrich, A. S. Borovik, J. Am. Chem. Soc. 2010, 132, 12188–12190.
- [34] K. Yamaguchi, S. Yamanaka, M. Nishino, Y. Takano, Y. Kitagawa, H. Nagao, Y. Yoshioka, *Theor. Chem. Acc.* **1999**, *102*, 328–345.
- [35] A. W. Addison, T. N. Rao, J. Reedijk, J. van Rijn, G. C. Verschoor, *J. Chem. Soc. Dalton Trans.* **1984**, 1349 1356.
- [36] N. Sun, L. V. Liu, A. Dey, A. G. Villar-Acevedo, J. A. Kovacs, M. Y. Darensbourg, K. O. Hodgson, B. Hedman, E. I. Solomon, *Inorg. Chem.* 2011, 50, 427–436.
- [37] D. M. P. Mingos, Struct. Bonding (Berlin) 2014, 153, 1-44.

Manuscript received: August 15, 2018

Accepted manuscript online: September 14, 2018

Version of record online: October 9, 2018